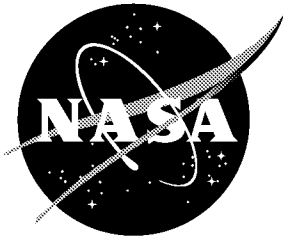# Numerical Simulation of a Spatially Evolving Supersonic Turbulent Boundary Layer

T. B. Gatski
Langley Research Center, Hampton, Virginia

G. Erlebacher
Florida State University, Tallahassee, Florida

Since its founding, NASA has been dedicated to the advancement of aeronautics and space science. The NASA Scientific and Technical Information (STI) Program Office plays a key part in helping NASA maintain this important role.

The NASA STI Program Office is operated by Langley Research Center, the lead center for NASA's scientific and technical information. The NASA STI Program Office provides access to the NASA STI Database, the largest collection of aeronautical and space science STI in the world. The Program Office is also NASA's institutional mechanism for disseminating the results of its research and development activities. These results are published by NASA in the NASA STI Report Series, which includes the following report types:

- TECHNICAL PUBLICATION. Reports of completed research or a major significant phase of research that present the results of NASA programs and include extensive data or theoretical analysis. Includes compilations of significant scientific and technical data and information deemed to be of continuing reference value. NASA counterpart and peer-reviewed formal professional papers, but having less stringent limitations on manuscript length and extent of graphic presentations.

- TECHNICAL MEMORANDUM. Scientific and technical findings that are preliminary or of specialized interest, e.g., quick release reports, working papers, and bibliographies that contain minimal annotation. Does not contain extensive analysis.

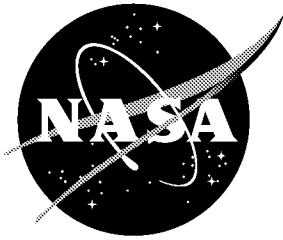- CONTRACTOR REPORT. Scientific and technical findings by NASA-sponsored contractors and grantees.

- CONFERENCE PUBLICATION. Collected papers from scientific and technical conferences, symposia, seminars, or other meetings sponsored or co-sponsored by NASA.

- SPECIAL PUBLICATION. Scientific, technical, or historical information from NASA programs, projects, and missions, often concerned with subjects having substantial public interest.

- TECHNICAL TRANSLATION. English-language translations of foreign scientific and technical material pertinent to NASA's mission.

Specialized services that complement the STI Program Office's diverse offerings include creating custom thesauri, building customized databases, organizing and publishing research results...even providing videos.

For more information about the NASA STI Program Office, see the following:

- Access the NASA STI Program Home Page at *http://www.sti.nasa.gov*

- E-mail your question via the Internet to help@sti.nasa.gov

- Fax your question to the NASA STI Help Desk at (301) 621–0134

- Phone the NASA STI Help Desk at (301) 621–0390

- Write to:
  NASA STI Help Desk
  NASA Center for AeroSpace Information
  7121 Standard Drive
  Hanover, MD 21076–1320

NASA/TM-2002-211934

Numerical Simulation of a Spatially Evolving Supersonic Turbulent Boundary Layer

T. B. Gatski
Langley Research Center, Hampton, Virginia

G. Erlebacher
Florida State University, Tallahassee, Florida

September 2002

Numerical simulation of a spatially evolving supersonic turbulent boundary layer

T. B. Gatski
Computational Modeling & Simulation Branch
NASA Langley Research Center, Hampton, VA 23681-2199
G. Erlebacher
Department of Mathematics
Florida State University, Tallahassee, FL 33206-4052

Abstract

The results from direct numerical simulations of a spatially evolving, supersonic, flat-plate turbulent boundary-layer flow, with free-stream Mach number of 2.25 are presented. The simulated flow field extends from a transition region, initiated by wall suction and blowing near the inflow boundary, into the fully turbulent regime. Distributions of mean and turbulent flow quantities are obtained and an analysis of these quantities is performed at a downstream station corresponding to $Re_x = 5.548 \times 10^6$ based on distance from the leading edge.

1. Introduction

Data from direct numerical simulations of turbulent shear flows are becoming an essential guide to the development of turbulent correlation closure models and the analysis of flow dynamics. In the incompressible regime, such simulations of turbulent channel (Mansour, Kim and Moin 1988) and boundary-layer (Moin et al. 1990) flows have been able to identify the relative distribution of the various terms in the Reynolds stress and dissipation rate budgets. In addition, analyses of the turbulent structures (Moser 1988, Moin and Moser 1989) in turbulent channel flow have also been made. These studies have significantly contributed to the understanding of turbulence physics as well as the development of improved turbulence models.

There has been and continues to be interest in the computation of turbulent compressible flows motivated by the optimal design of high-speed vehicles and associated propulsion systems. Databases of turbulent flows, which are more commonly available in the incompressible regime, have not been as widespread for supersonic compressible flows; however, numerical simulations of such supersonic flows have been performed (Rai, Gatski and Erlebacher 1995, Coleman, Kim and Moser 1995, Guarini et al. 2000, and Maeder, Adams and Kleiser 2001).

The direct numerical simulation (DNS) presented here is of a turbulent, supersonic, zero pressure gradient, flat plate boundary layer flow with a free-stream Mach number $M_\infty = 2.25$ and a free-stream Reynolds number $Re_\theta \approx 4.25 \times 10^3$. Unlike previous boundary-layer studies (Coleman, Kim and Moser 1995, Guarini et al. 2000, and Maeder, Adams and Kleiser 2001), the numerical simulation is a fully spatially evolving boundary-layer flow with an inflow boundary located in the laminar regime, and transition is forced through wall suction and blowing. The conditions closely approximate the experiment of Shutts, Hartwig and Weiler (1977), Case 55010501. A

1

flow with this large a value of free-stream Re_θ can be simulated because of the dependence of viscosity on temperature. Under the adiabatic conditions of the experiment, the temperature increases as the wall is approached and the Re_θ based on local conditions is correspondingly reduced. Thus, in regions near the wall where resolution requirements are the most stringent, the increased viscosity effectively reduces the grid density required to compute the flow.

The computational method used in this study is a high-order accurate, upwind-biased, implicit, finite-difference method that was developed (Rai and Moin 1991, 1993) and used to compute transition to turbulence on a flat plate with a low Mach number ($M_\infty = 0.1$), and subject to high free-stream disturbance levels. The technique involves using upwind-biased differences for the convective terms, central differences for the viscous terms, and an iterative-implicit time integration scheme. The computational method (Rai and Moin 1991) uses the nonconservative form of the governing equations to obtain the solution. Therefore, this approach is confined to flows that do not contain discontinuities (shocks). In the present flat plate simulation, the free stream Mach number is assumed to be sufficiently low to preclude eddy-shocklets. The computed results confirm this assumption.

Results obtained in the fully turbulent region at a distance of $x = 8.8$ units downstream of the leading edge are analyzed. This location corresponds to a Re_x of 5.548×10^6 and an $Re_\theta = U_\infty \theta / \nu_\infty \approx 4.25 \times 10^3$ (or a wall momentum thickness Reynolds number $Re_{\theta w} = U_\infty \theta / \nu_w \approx 1.343 \times 10^3$). Profiles of various mean velocity and thermal variables, as well as turbulent velocity and thermal variables, are discussed.

2.   Problem Formulation and Numerical Solution

The numerical procedure used in the direct simulations presented here is described in detail in Rai, Gatski and Erlebacher (1995). As noted in the previous section, an important limitation imposed by using a nonconservative formulation of the governing equations is that the method can only be used to compute flows that are free of flow discontinuities (such as purely subsonic flows). The nonconservative formulation of the governing equations was chosen for this investigation because of the efficiency of the approach, the availability of a validated computer program that uses the approach, and because the flow does not exhibit discontinuities. The present method is second-order accurate in time and fourth-order accurate in space.

The computational region of interest is shown in Fig. 1. In the streamwise x-direction, it extends from $x = 4.0$ to $x = 15.0$ for the turbulence simulation. (Note that all spatial distances have been normalized by unit length.) The grid spacing in the streamwise direction is sufficiently fine to resolve the flow features of interest up to $x = 9.0$. Thereafter, the grid gradually becomes very coarse so that the disturbances in the boundary layer rapidly attenuate and a simple boundary condition can be used at the exit boundary. The dimensions of the computational region in the wall normal y- and spanwise z-directions are 3.0 and 0.35, respectively. As Fig. 1 shows, the boundaries of the computational region consist of the inlet boundary, the exit boundary, the lower surface solid boundary, the upper surface symmetry boundary,
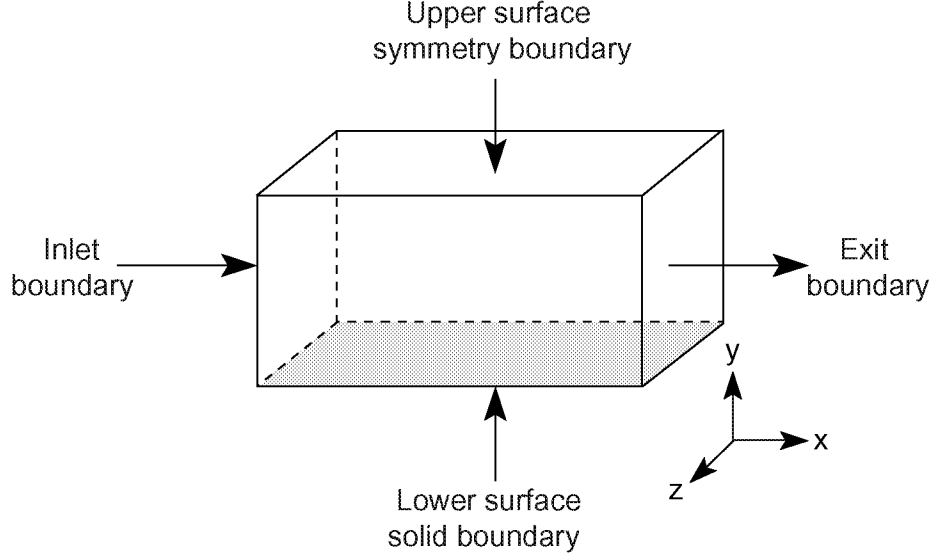
Figure 1. Sketch of computational domain (not to scale).

and the two boundaries in the spanwise direction. The boundary conditions used at each of these boundaries are as follows.

Inlet Boundary

The inlet boundary is comprised mainly of a supersonic flow except for the subsonic portion of the boundary layer. The values of all the dependent variables are fixed at this boundary, and obtained from a similarity compressible boundary-layer solution).

Exit Boundary

The exit boundary is a supersonic exit boundary except for the subsonic portion of the boundary layer. All the variables are extrapolated from the interior to the exit boundary for those exit boundary points where the flow Mach number is greater than unity. For boundary points where the streamwise Mach number is subsonic, the extrapolation process is implemented for all the variables except the pressure. The pressure is set equal to the pressure at the grid point at which the Mach number first becomes supersonic. To be accurate, this approximation requires that the disturbances in the boundary layer be attenuated before the exit boundary is reached. As described previously, this attenuation is accomplished by using a grid that gradually becomes very coarse (geometric stretching) in the streamwise direction as the exit boundary is approached.

Upper Surface and Spanwise Boundaries

A symmetry boundary condition is used at the upper surface boundary. This boundary condition corresponds to the one used for a channel flow simulation rather than a flat-plate simulation. However, the ratio of the width of the channel to the momentum thickness at $x = 9.0$ is about 300. Therefore, the computed solution would be very close to a flat plate solution. Additionally, the grid coarsens in the y-direction so that disturbances are attenuated before they reach the upper boundary.

3

A periodic boundary condition is used in the spanwise direction. The width of the computational region in the spanwise direction was determined with the help of two-point correlations of the velocity components in this direction obtained with coarse grids and wider domains. The width $L_z = 0.35$ was chosen such that the auto-correlation coefficient values were sufficiently small ($\mathcal{O}(10^{-2})$) at the tail end of the correlation curve.

Lower Surface Solid Boundary
The lower boundary of the computational domain corresponds to the plate surface. Except for the portion of the plate where blowing and suction are implemented, a no-slip boundary condition together and a temperature condition (isothermal wall temperature) is specified. The dependent variables are obtained from

$$u_{(1)} = v_{(1)} = w_{(1)} = 0, \quad T_{(1)} = T_w, \quad p_{(1)} = p_{(2)} \tag{1}$$

where the subscripts (1) and (2) correspond to the wall and the first point away from the wall, respectively. The density at the wall is computed by using the pressure and the temperature. In the region of wall blowing and suction (in this computation, $4.5 \le x \le 5.0$) the normal component of the velocity is computed as

$$v_1 = \mathcal{A} u_\infty f(x) g(z) h(t) \tag{2}$$

where

$$
\begin{aligned}
f(x) &= 4\sin\theta(1-\cos\theta)/\sqrt{27} \\
\theta &= 2\pi(x - x_a)/(x_b - x_a) \\
g(z) &= \sum_{l=0}^{l_{max}} Z_l \sin(2\pi l(z/z_{max} + \phi_l)) \\
\sum_{l=0}^{l_{max}} Z_l &= 1, \quad Z_l = 1.25 Z_{l+1} \\
h(t) &= \sum_{m=1}^{m_{max}} T'_m \sin(2\pi(\beta t + \phi_m)) \\
\sum_{m=1}^{m_{max}} T'_m &= 1, \quad T'_m = 1.25 T'_{m+1}
\end{aligned}
\tag{3}
$$

where $l_{max} = 10$, $m_{max} = 5$, $x_a = 4.5$ and $x_b = 5.5$ are the streamwise locations of the beginning and the end of the blowing/suction strip, respectively, $\mathcal{A}$ is the amplitude of the imposed disturbance (0.04), β is the fundamental temporal frequency of the disturbance (75000 Hz), ϕ_l and ϕ_m are random numbers ranging between 0.0 and 1.0, and z_{max} is the dimension (0.35) of the computational region in the spanwise direction.

The numerical method and boundary conditions just discussed were validated by studying the evolution of two-dimensional, small amplitude disturbances in a flat-plate flow at a Mach number of 4.5 and a free-stream temperature of 110° R, with a unit Reynolds number based on free-stream conditions of 83333. It was shown in

Rai, Gatski and Erlebacher (1995) that the streamwise evolution of the disturbance amplitude maxima computed with the present methodology was in excellent agreement with parabolized stability equation results. With the success of this small amplitude disturbance study, the methodology was then applied to the forced, flat-plate supersonic boundary-layer flow.

The results reported by Rai, Gatski and Erlebacher (1995) were obtained in several stages by interpolating an initial solution from an extremely coarse grid onto successively finer grids. The computation on each of the intermediate grids was carried to a point where the skin-friction distribution (after spanwise averaging) showed minor changes in time and exhibited a time average that was essentially in equilibrium. In their study, these results were mapped onto the finer grid $(N_x \times N_y \times N_z) = (1701 \times 55 \times 501)$ used in this study and allowed to evolve until the transients from the mapping process disappeared.

To help assess the accuracy of the numerical simulation, one-dimensional spectra of the primitive variables were examined in the periodic z-direction. At a given x-station along the solid boundary and a y-value in the boundary layer, the corresponding two-point correlation function can be formed in the homogeneous z-direction, and is given by

$$R_{\alpha\alpha}(r_z) = \sum_{k=1}^{N_z-1} \alpha_k \alpha_{k+k_r}, \qquad k_r = 0, 1, \ldots, k-1, \tag{4}$$

where $r_z = k_r \Delta z$, N_z is the number of grid points in the z-direction, and α represents any one of the primitive variables $\rho,$, u, v, w, or p. (Note that the periodicity allows the two-point correlation function to be obtained over the whole range of z grid points.) The discrete power spectrum is then obtained from Eq. (4) as

$$E_{\alpha\alpha}(k_z \Delta z) = 1 + 2 \sum_{k_r=1}^{(N_z-1)/2} R_{\alpha\alpha}(k_r \Delta z) \cos\left(\frac{2\pi n k_r}{N_z - 1}\right), \qquad n = 0, \ldots, \frac{(N_z - 1)}{2}, \tag{5}$$

where $k_z \Delta z = n/(N_z - 1)$, and $\Delta z = L_z/(N_z - 1)$. Figure 2 shows the normalized spectra for the primitive variables in the homogeneous z-direction at three different y^+ locations. (As will be discussed further in Sec. 3., these results are obtained at a downstream station corresponding to $Re_x = 5.548 \times 10^6$, or $x = 8.8$ units from the leading edge.) The wall normal distances correspond to an inner layer location where the mean velocity is linear ($y^+ \leq 5$), a location just at the beginning of the log-layer region ($y^+ = 27$), and a location in the outer layer at the beginning of the wake region ($y^+ = 184$). The spanwise wavenumber is normalized by the boundary-layer thickness δ_c at which the van Driest velocity is $\sqrt{\gamma} M_\infty$. As Fig. 2 shows, with the exception of the E_{vv} component at $y^+ = 5$, spectral amplitude decreases at least three decades between the lowest and highest wavenumbers for both the velocity and thermal variables. However, the v-energy component exhibits an increase at $k_z \delta_c \approx 15$ and the overall decrease is closer to two orders of magnitude. The peak in the E_{vv} spectrum suggests a periodic v-velocity component in the spanwise direction that characterizes the spanwise vortices imbedded within the boundary layer. The wavelengths corresponding to the E_{vv} peak at $y^+ = 5$ and 27 are $\lambda_z^+ \approx 100$ and
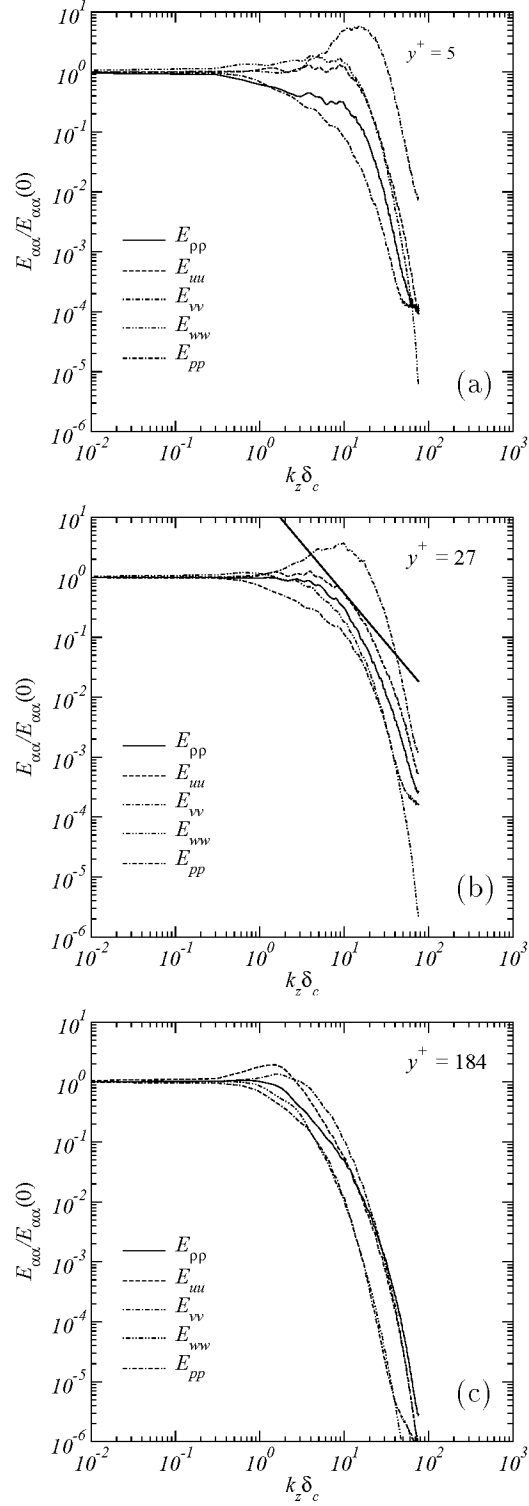
5

Figure 2. Normalized power spectrum of the primitive variables in the homogeneous z-direction at $y^+ = 5$, 27, and 184: (b) ——, $-5/3$ law.

50, respectively. These values of λ_z^+ are consistent with experimental results (see Smits and Dussauge 1996) that show the spanwise spacing of streaks in the boundary layer to have a mean spacing of $\lambda_z^+ = 100$. A further validation of the simulation can be found in the estimate of the high wavenumber limit of η/λ_z (where η is the Kolmogorov length scale and $\lambda_z = 2\pi k_z$). At $y+ = 27$, $\eta\lambda_{z\max}$ is approximately 0.72, which can be interpreted as a measure of the relative size of the Kolmogorov scale to the spanwise (grid) resolution. While resolution down to the Kolmogorov scales is desirable, practical constraints on such a spatial resolution prevents this.

As Fig. 2(b) shows, only a small spectral region is consistent with the $-5/3$ slope. Although other results clearly show a log-law region that equilibrium between production and dissipation, the relatively low Reynolds number of this flow precludes a large inertial region in the spectrum and precludes a large region where turbulent energy and dissipation rate balance.

Another assessment of the computational accuracy of the simulation is provided by the two-point correlation function given by Eq. (4). Figure 3 shows the spanwise variation of the correlation coefficients for both the turbulent velocity and thermal variables. This distribution can be used to assess whether the computational domain in the spanwise direction is sufficiently wide to accommodate the turbulence dynamics. A measure of the effect is to ensure that the two-point correlation function is sufficiently decorrelated over distances $L_z/2$ ($= 0.175 \approx 1.63\delta_c$). Figure 3 shows that at the $y^+ = 5$ and 27 all the turbulent variables have been sufficiently decorrelated over distances much less than $L_z/2$. At $y^+ = 184$ the migrations about zero are slightly larger, although such migrations are relatively constant for $r_z > 0.8\delta_c$.

The separation distances at which the minimums in the velocity correlation coefficients occur can provide some insight into the compressible turbulent boundary layer structure (Kim, Moin and Moser 1987). An estimate of the separation between the low- and high-speed streaks can be obtained from the $R_{uu}(r_z)/R_{uu}(0)$ autocorrelation. At $y^+ = 5$, shown in Fig. 3(a), $R_{uu}(r_z)/R_{uu}(0)$ has a minimum at $r_z/\delta_c \approx 0.048$ ($r_z^+ \approx 50$) which is an estimate of the mean spacing between the high- and low-speed fluid at this $y+$ location. Similarly, some estimate of the size of any streamwise vortical structures can be obtained from $R_{vv}(r_z)/R_{vv}(0)$. As shown in Fig. 3(a), where $y^+ = 5$, the minimum in the $R_{vv}(r_z)/R_{vv}(0)$ distribution occurs at $r_z/\delta_c \approx 0.026$ ($r_z^+ \approx 27$). This separation distance then corresponds to an estimate of the mean diameter of a streamwise vortex. Interestingly, both these results are consistent with the incompressible channel flow results obtained by Kim, Moin and Moser (1987) and suggest that, at least in close proximity to the wall, the structure of the compressible turbulent boundary is similar to the structure in an incompressible flow.

3. Results

The problem under investigation is based on the parameter range of the supersonic boundary layer experiment of Shutts, Hartwig and Weiler (1977). In the physical experiment, the inlet Mach number was 2.25 and the unit Reynolds number ($Re/$in.) based on inlet conditions was 6.35×10^5. The free-stream temperature was 305° R and the adiabatic wall temperature was 580° R.
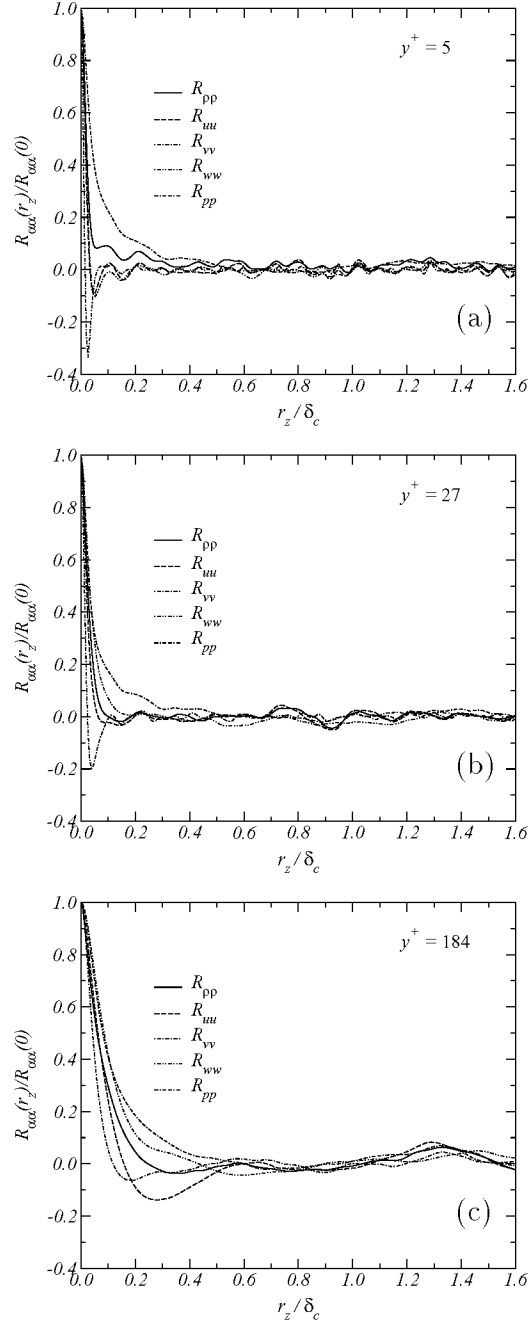
7

Figure 3. Normalized two-point correlation tensor in the homogeneous z-direction at $y^+ = 5$, 27, and 184.

In the computational experiment, the domain consists of three regions. The first region is fairly well resolved and contains the region of blowing and suction and some of the end stage transition phenomena, $2.54 \times 10^6 \lesssim Re_x \lesssim 4.42 \times 10^6$ (where Re is based on values at the boundary layer edge). The second region also contains some of the end stage transition phenomena as well as the turbulent portion of the flow field,

8

$4.42 \times 10^6 \lesssim Re_x \lesssim 5.67 \times 10^6$, and has the densest grid in the computational domain. The third region is discretized by using a grid that gradually becomes very coarse in the streamwise direction, $5.67 \times 10^6 \lesssim Re_x \lesssim 9.46 \times 10^6$. The total number of grid points used in the computation is approximately 47 million ($1701 \times 55 \times 501$ grid). Unless otherwise stated, the results presented here were determined at the x-station corresponding to $Re_x = 5.548 \times 10^6$ ($x = 8.8$). Based on the wall shear velocity at this location, the resolution in the resolved (second) turbulent region is $\Delta x^+ = 13.9$ and $\Delta z^+ = 6.8$ and the first grid point off the wall is at $y^+ = 0.97$. The boundary layer thickness (based on 99.5 percent of the free-stream velocity) at $Re_x = 5.548 \times 10^6$ is approximately 1.03×10^3 wall units.

Figure 4 shows the computed skin-friction distribution compared with a theoretical estimate for the fully turbulent regime given by (see White 1974, p. 644 for details)

$$C_f = \left(\frac{0.455}{\mathrm{S}^2} \right) \left[\ln \left(\frac{0.06}{\mathrm{S}} Re_x \frac{\bar{\mu}_\infty}{\bar{\mu}_w} \sqrt{\frac{\overline{T}_\infty}{\overline{T}_w}} \right) \right]^{-2}, \tag{6}$$

where $\overline{T}$ is the mean temperature, $\bar{\mu}$ is the viscosity of the fluid, Re_x is the Reynolds number based on free-stream conditions, and by

$$\mathrm{S} = \frac{1}{\sin^{-1}\mathrm{A}} \sqrt{\frac{\overline{T}_w}{\overline{T}_\infty} - 1}, \quad \text{with} \quad \mathrm{A} = \left(\frac{\gamma - 1}{2} M_\infty^2 \frac{\overline{T}_\infty}{\overline{T}_w} \right)^{1/2}. \tag{7}$$

The region of blowing and suction can be observed in the region $2.8 \times 10^6 \lesssim Re_x \lesssim 3.1 \times 10^6$ as small variations in the computed skin-friction. Further downstream, in the end stage transition region, the skin-friction increases dramatically, reaches a maximum and then begins to decrease. As shown in Fig. 4, this streamwise development (slope) is coincident with the results predicted by Eq. (6).

Figure 5 shows the computed van Driest velocity

$$U_c = \int_0^U \sqrt{\frac{\rho}{\rho_w}} dU. \tag{8}$$

normalized by the wall-shear velocity and plotted as a function of the wall normal distance (in wall units) at the streamwise location $x = 8.8$. This location is at a distance of approximately 11 boundary layer thicknesses downstream of the end of transition. Also plotted in Fig. 5 are the curves $U_c^+ = y^+$ and the log-law $U_c^+ = \kappa^{-1} \ln(y^+) + 5.1$ ($\kappa = 0.41$). The simulation results agree very well with both the asymptotic behavior near the wall and the log-law results.

The corresponding variation across the boundary layer of the mean density, pressure, and temperature variables is shown in Fig. 6. Both the mean pressure $\overline{p}$ and total temperature $\overline{T}_t$ are constant in the inner layer of the boundary layer, but $\overline{T}_t$ increases slightly near the outer edge of the boundary layer. The mean density $\overline{\rho}$ increases across the layer by nearly a factor of two, and the mean temperature $\overline{T}$ decreases by approximately a factor of two across the layer.
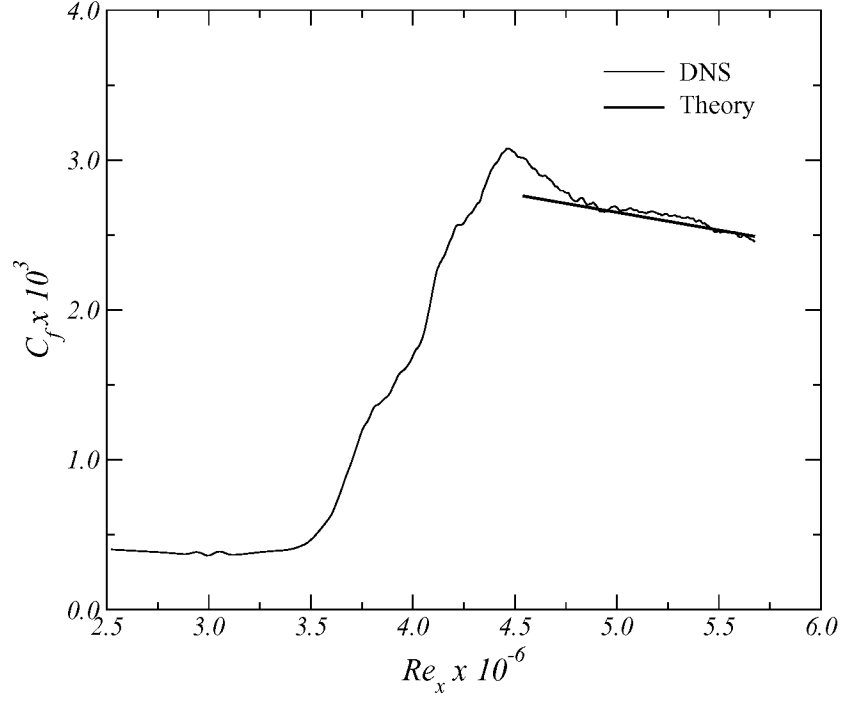
9

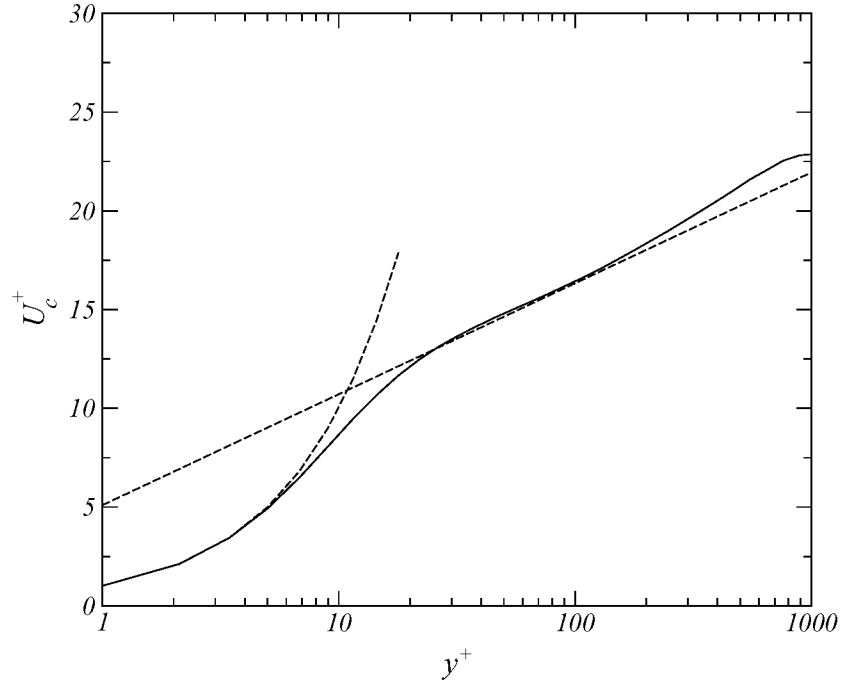Figure 4. Streamwise variation of skin-friction coefficient: Theory from Eq. (6).

Figure 5. Van Driest mean velocity distribution across boundary layer. Solid line DNS, and dashed lines represent $U_c^+ = y^+$ and $U_c^+ = \kappa^1 \ln(y^+) + 5.1$ in the near-wall and log-layer regions, respectively.
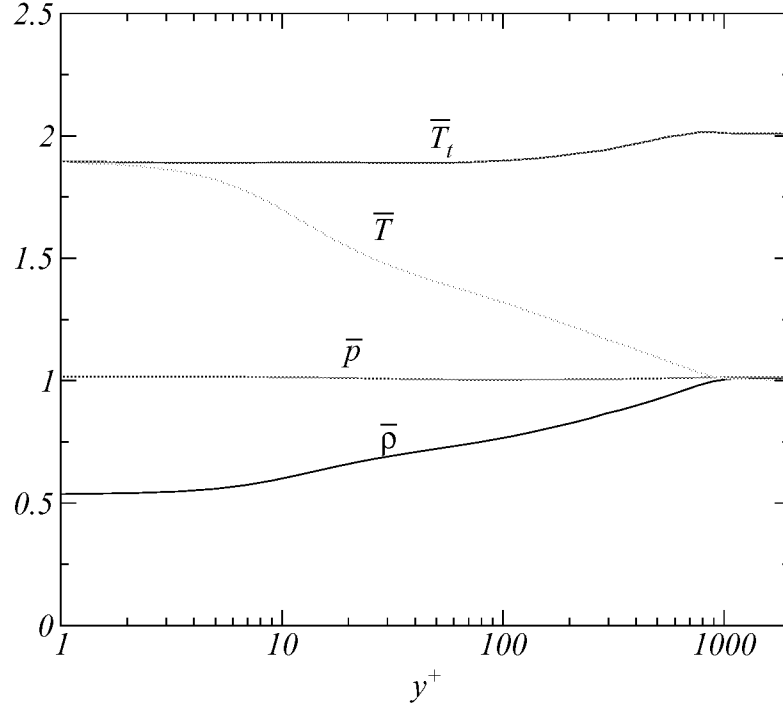
Figure 6. Variation of mean thermodynamic variables across boundary layer.

With the behavior of the mean velocity and thermal fields across the boundary layer separately established, the question arises whether their coupled behavior is being properly represented. The coupling of the mean thermal and velocity fields is the basis of the Reynolds analogy postulated over 100 years ago. One such measure is the Crocco-Busemann relation (White 1974) which can be written for the current simulation as

$$\frac{\overline{T}}{\overline{T}_e} \approx \frac{T_{aw}}{\overline{T}_e} - \frac{U^2}{2c_p\overline{T}_e},$$ (9)

where $\overline{T}_e$ is the mean boundary-layer edge temperature, and the isothermal wall temperature boundary condition is $T_w = T_{aw}$. Note that the recovery factor r is often included in the last term of Eq. (9); however, since this equation is derived under the assumption that the turbulent Prandtl number is $Pr_t \approx 1$ ($r \approx Pr_t^{2/3}$), the recovery factor was set to unity. Figure 7 shows the DNS data for the temperature ratio $\overline{T}/\overline{T}_e$ as a function of U/U_e across the boundary layer for compariosn with the theoretical predictions of Eq. (9). The figure shows very good agreement between the two quantities across most of the boundary layer. Only in the outer layer, where many of the assumptions used in the derivation of Eq. (9) become invalid, do the simulation and theoretical results deviate.

Figure 8(a) shows the behavior of the scaled Reynolds shear stress across the boundary layer, and Fig. 8(b) shows the behavior of the corresponding total stress. The scaling used in the figure is motivated by Morkovin's hypothesis (Morkovin 1964) which simply states that the "...*essential dynamics of these supersonic shear flows will*
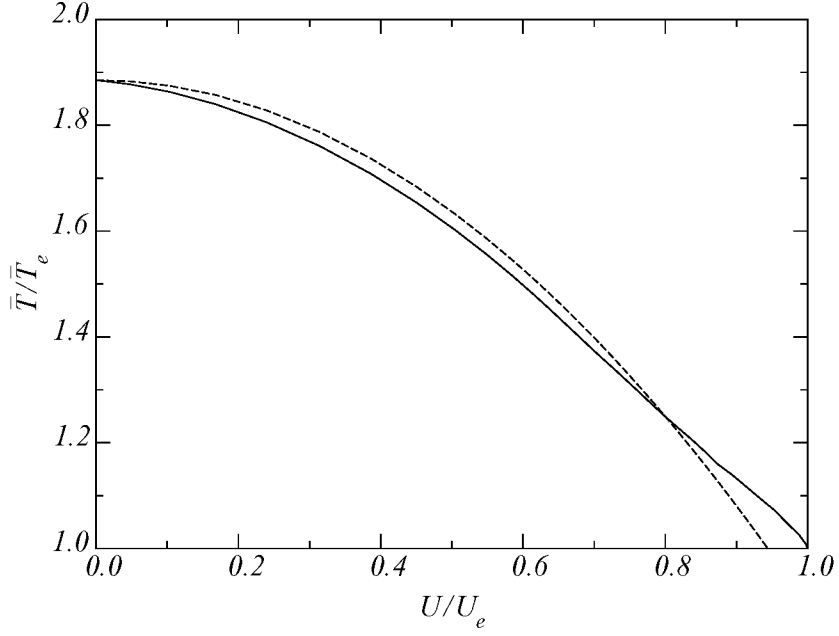
11

Figure 7. Mean temperature distribution across boundary layer and comparison with the Crocco-Busemann relation (dashed line).

follow the incompressible form..." This observation was quantified by the proposal that

$$\left(\frac{\overline{\rho}}{\overline{\rho}_w}\right)\frac{\overline{uv}}{u_\tau^2}, \qquad \left(\frac{\overline{\rho}}{\overline{\rho}_w}\right)\frac{\overline{u^2}}{u_\tau^2} \tag{10}$$

"would depend little on Mach number ..." The Reynolds normal stresses are shown in
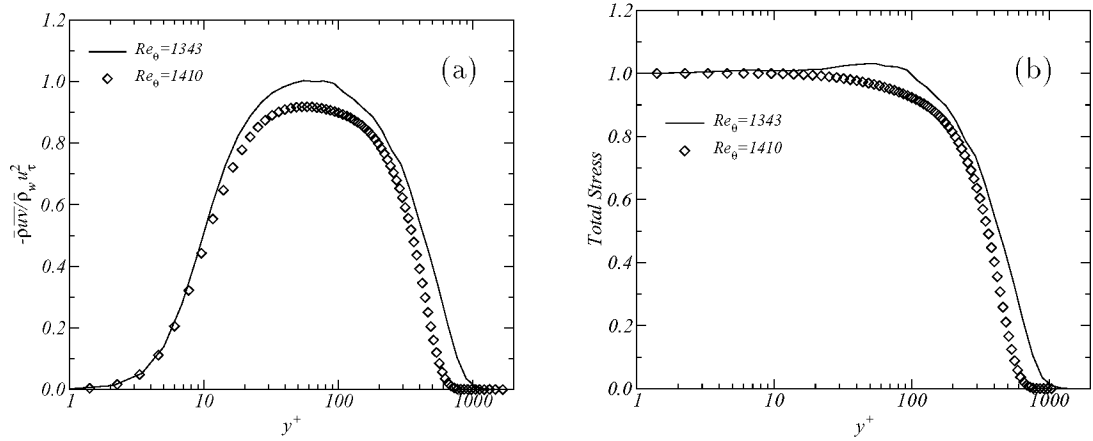

Figure 8. Shear stress distribution across boundary layer: (a) scaled Reynolds shear stress; (b) total shear stress. Symbol represents incompressible DNS (Spalart 1988), and solid line represents current compressible simulation.

12

Fig. 9. It is useful to compare these results with some incompressible data in order
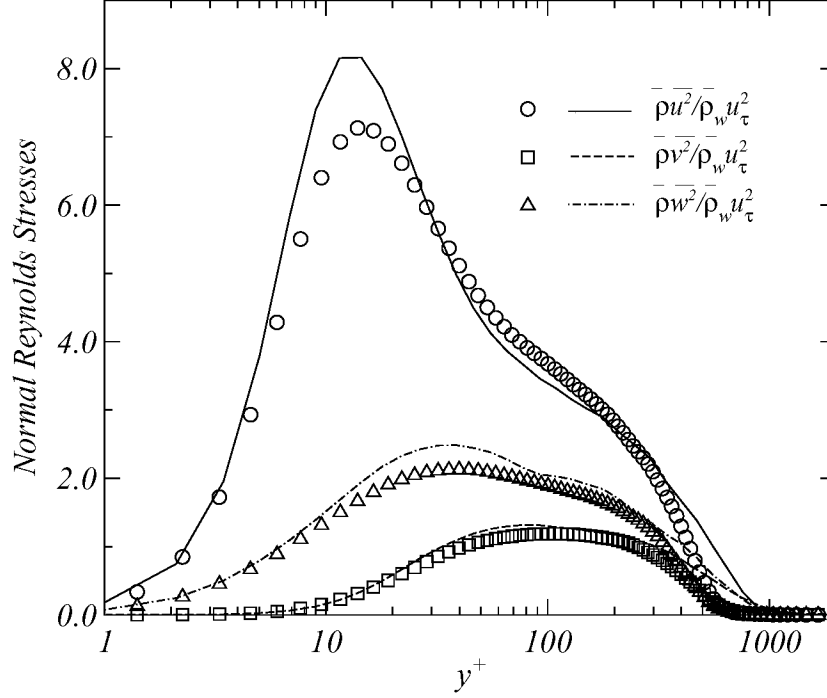

Figure 9. Reynolds normal stress distribution across boundary layer. Symbols represents incompressible DNS (Spalart 1988) at $Re_\theta = 1410$. Solid and dashed lines are current compressible simulation.

to assess the applicability of Morkovin's hypothesis and to help validate the present DNS data. At the $Re_x = 5.548 \times 10^6$ ($x = 8.8$) streamwise station shown here, the free-stream momentum thickness Reynolds number $Re_\theta = (U_\infty \theta / \nu_\infty)$ is $\approx 1.25 \times 10^3$. This corresponds to a wall momentum thickness Reynolds number $Re_{\theta w} = (U_\infty \theta / \nu_w)$ $\approx 1.343 \times 10^3$. Fortunately, incompressible data exists in this Reynolds number range and can be used for comparison. Also shown on Figs. 8 and 9 are the incompressible simulation data of Spalart (1988) at $Re_\theta = 1410$. The results from both the shear stress and streamwise normal stress from the current simulation are larger than the corresponding incompressible results, particularly in the region of peak values. The spanwise normal stress components, $\overline{\rho w^2}/\overline{\rho}_w u_\tau^2$ from both simulations are similar; however, the transverse components, $\overline{\rho v^2}/\overline{\rho}_w u_\tau^2$ also show that the incompressible results are less than the corresponding compressible data.

From the comparison with the incompressible results, the behavior of the shear stress, particularly the peak value, is of concern. Although it can be shown in the case of fully developed channel flow that the total stress (turbulent plus viscous) expressed in wall units cannot exceed unity, the case of the developing boundary layer is less clear. Expressed in wall units, the streamwise mean momentum equation for this zero

pressure gradient flow can be written as

$$\left(\frac{\bar{\rho}}{\bar{\rho}_w}\right)\left(U^+\frac{\partial U^+}{\partial x^+} + V^+\frac{\partial U^+}{\partial y^+}\right) = \frac{\partial}{\partial y^+}\left[-\left(\frac{\bar{\rho}}{\bar{\rho}_w}\right)\overline{uv}^+ + \left(\frac{\bar{\mu}}{\bar{\mu}_w}\right)\bar{\sigma}_{xy}^+\right], \qquad (11)$$

where $\bar{\sigma}_{xy}^+$ is the mean viscous stress. Note that the mean density and mean dynamic viscosity ratios appear due to the wall unit scaling that uses the wall values for $\bar{\rho}_w$ and $\bar{\mu}_w$ ($\bar{\nu}_w$). Since the left hand side of Eq. (11) is small but not negligible, no definite statements can be made about the distribution of the total stress across the boundary layer. (Recall that for incompressible channel flow the total stress varies linearly across the channel.) Nevertheless, as Fig. 8(b) shows, the incompressible simulation yields a relatively constant total stress level up to a y^+ value ≈ 15 and then decays monotonically with increasing distance to the wall. The compressible simulation displays the same trend in the inner layer region as the incompressible data; however, in the log-layer region the total stress exceeds unity, increasing slightly and then decreases monotonically as the boundary layer edge is approached. While Morkovin's hypothesis may not apply directly to the behavior of the total stress distribution across the boundary layer, the results shown in Fig. 8(b) suggest that the deviation between the incompressible and compressible results may be due to inaccuracies in the compressible simulation. Further simulations are ongoing (Pirozzoli, Grasso and Gatski 2002)with a different numerical algorithm and grid structure that will hopefully shed light on this issue.

Turbulent fluctuations of the thermodynamic variables ρ, p, T, and (total temperature) T_t are not negligible in such boundary layer flows. Figure 10 shows the distribution of these variables across the boundary layer. The pressure fluctuation
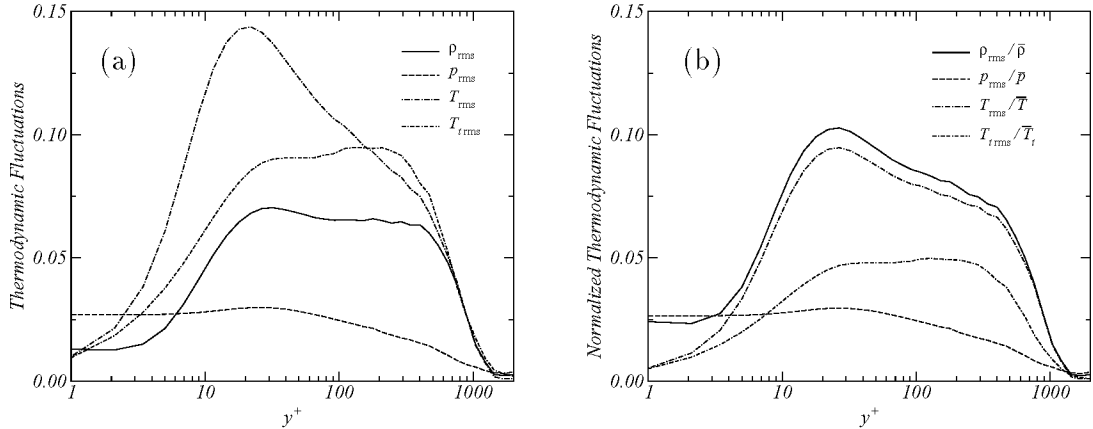

Figure 10. Distribution of root mean square fluctuations of thermodynamic variables across boundary layer: (a) non-dimensionalized with free-stream values; (b) normalized with local mean values.

levels are relatively constant throughout the inner-layer including most of the log-layer region (cf. Fig. 5). As distance from the wall increases, the pressure fluctuation

levels decline further (from $\approx$ 2 percent of the mean). Since the mean pressure across the boundary layer is relatively constant, the free-stream and local mean scaling have very few differences. In the near-wall region, the density fluctuations are also relatively constant and similar to the corresponding behavior displayed by the mean density shown in Fig. 6. Farther from the wall, the density fluctuations reach a new, higher plateau (Fig. 10(a)) across the log-layer and a portion of the outer layer. In contrast, the normalized density fluctuations (Fig. 10(b)) reach a peak near $y^+ = 20$ and then decrease with increasing distance from the wall.

As expected, the behavior of the temperature and total temperature root mean square (rms) fluctuations are comparable in the near-wall region with both quantities increasing linearly with y^+. The temperature fluctuations reach a peak value near $y^+ = 20$ and are about 15 percent of the free-stream mean value. With increasing distance from the wall these temperature fluctuations decrease. The same trend is exhibited with the normalized temperature fluctuations, although the intensity levels are decreased due to local mean temperature exceeding unity across the boundary layer (see Fig. 6). Since the mean total temperature is relatively constant and greater than unity across the boundary layer, both the free-stream and local mean scaling yield qualitatively similar results with only the magnitudes decreasing in the normalized case. The total temperature fluctuation levels reach $\approx$ 5 percent of the local mean value.

Compressible turbulent dilatation effects, such as dilatation dissipation and pressure-dilatation, do not play a role in wall-bounded flows (Sarkar 1995). Previous models (see Gatski 1996) of dilatation dissipation, for example, have assumed a ratio of $\varepsilon_d/\varepsilon_s \sim \mathcal{O}(M_t^2)$. Figure 11 shows the dependence of $\varepsilon_d/\varepsilon_s$ on M_t across the boundary layer. Homogeneous forms of both the dilatation dissipation ε_d and solenoidal dissipation ε_s have been used and are given by (Sarkar et al. 1991)

$$\overline{\rho}\varepsilon_d = \frac{4}{3}\overline{\mu}\overline{u_{k,k}^2} \text{ and } \overline{\rho}\varepsilon_s = \overline{\mu\omega_i\omega_i} \tag{12}$$

where ω_i is the fluctuating vorticity vector. As Fig. 11(b) shows, the turbulent Mach number reaches a peak value of $\approx$ 0.25, whereas the ratio $\varepsilon_d/\varepsilon_s$ obtained from the simulation data at the corresponding M_t is only $\approx 3 \times 10^{-4}$. These results show that such models are inadequate for wall-bounded flows and that the dilatation dissipation does not contribute significantly to total turbulent dissipation rate.

4. Conclusions

A direct numerical simulation of a spatially evolving, supersonic turbulent boundary layer flow has been described. A fourth-order accurate, upwind-biased, implicit, finite-difference method with second-order temporal accuracy has been used in the simulation. Power spectra and two-point correlation data have been analyzed to help assess the numerical accuracy of the computation. With the exception of the v-power spectrum component, these results showed a three order of magnitude decay of the power spectral amplitudes across the wavenumber range examined. In addition, the decorrelation of the spanwise two-point correlations confirmed that the domain size
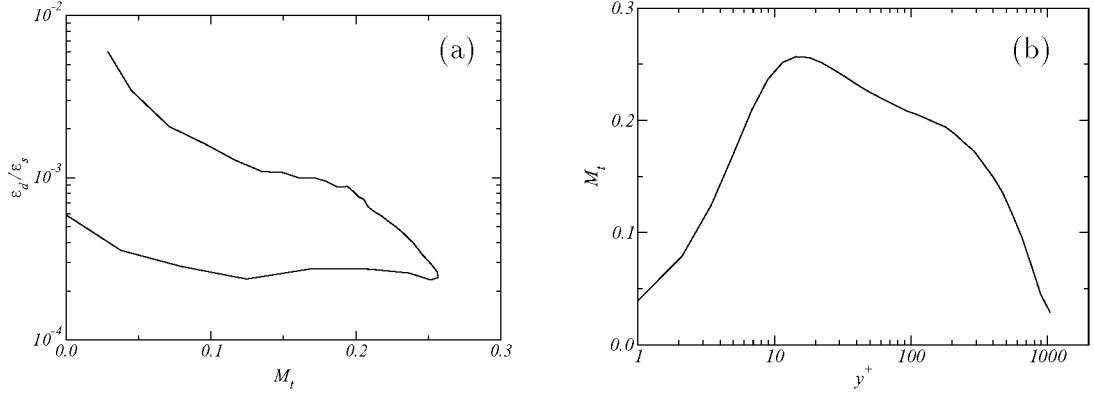
15

Figure 11. Influence of dilatation dissipation across boundary layer: (a) ratio of dilatation to solenoidal dissipation as a function of turbulent Mach number; (b) turbulent Mach number variation across boundary layer.

in the z-direction was sufficiently large and did not have any adverse impact on the current simulation.

Both the skin friction variation in the streamwise direction and the van Driest velocity in the fully turbulent regime agreed quite well with the corresponding analytical models. The slope of the skin-friction decay in the fully turbulent region was consistent with previous theory, and both the near-wall asymptotic behavior and log-law were well replicated by the van Driest velocity in the fully turbulent region as well.

The mean turbulent thermal field variables were relatively constant in the near-wall region. As distance from the wall increased, the mean density and temperature fields showed a corresponding increase and decrease, respectively, across the layer. The mean pressure and total temperature remained relatively constant across the entire layer.

Unfortunately, the turbulent shear stress and streamwise normal stress component obtained from the simulation data appear to have peak values that are too high when compared with incompressible simulation data at similar values of Re_θ. This result, and the relatively low supersonic Mach number, indicate that Morkovin's hypothesis should be applicable.

Root mean square (rms) distributions of the turbulent thermal fluctuations showed that the temperature fluctuation levels can reach as high as 15 percent of the free-stream mean value in the inner part of the boundary layer; however, when normalized with respect to the local mean, such disturbances are about 9 percent of the mean. In contrast, rms density fluctuations are found to have maximum levels that are about 7 percent of the free-stream mean; whereas, when scaled with the local mean value these fluctuation levels are about 10% of the mean. Total temperature fluctuations display the same qualitative behavior as the temperature fluctuations; however, the maximum fluctuation levels, when scaled with the free-stream, are about 10 percent, and the local mean scaling yields values in the range of 5 percent. Since the mean pressure

16

distribution was constant across the boundary layer, the relative fluctuation levels retain the same relative behavior, whether scaled by the free-tream or local mean values. In both cases, the maximum fluctuation levles correspond to approximately 2.5 percent of the mean.

References

Coleman G. N., Kim, J. and Moser R.D. 1995 "A numerical study of turbulent supersonic isothermal-wall channel flow," *J. Fluid Mech.* **305**, 159–183.

Gatski, T. B. (1996) "Turbulent flows: model equations and solution methodology," In *Handbook of Computational Fluid Mechanics*, (R. Peyret, Ed.), Academic Press.

Guarini, S. E., Moser, R. D., Shariff, K., and Wray, A. 2000 "Direct numerical simulation of a supersonic turbulent boundary layer at Mach 2.5." *J. Fluid Mech.*, **414**, 1–33.

Kim, J., Moin, P., and Moser, R. 1987 "Turbulence statistics in fully developed channel flow at low Reynolds number," *J. Fluid Mech.*, **177**, 133–166.

Maeder, T., Adams, N. A., and Kleiser, L. 2001 "Direct simulation of turbulent supersonic boundary layers by an extended temporal approach," *J. Fluid Mech.*, **429**, 187–216.

Mansour, N. N., Kim. J., and Moin P. 1988 "Reynolds-stress and dissipation rate budgets in a turbulent channel flow." *J. Fluid Mech.* **194**, 15–44.

Moin, P., and Moser, R. D. 1989 "Characteristic–eddy decomposition of turbulence in a channel," *J. Fluid Mech.*, **200**, 471–509.

Moin, P., Shih, T.-H., Driver, D. and Mansour, N. N. 1990 "Direct numerical simulation of a three-dimensional turbulent boundary layers," *Phys. Fluids A* **2**, 1846–1853.

Morkovin, M. V. 1964 "Effects of compressibility on turbulent flows," In *The Mechanics of Turbulence* (A. Favre, ed.), Gordon and Breach, New York, 367–380.

Moser, R. D. 1988 "Statistical analysis of near-wall structures in turbulent channel flow," *Proc. Zaric Memorial Intl. Seminar on Wall Turbulence*, Dubrovnik, Yugoslavia, May 16–20.

Pirozzoli, S., Grasso, F., and Gatski, T. B. 2002 "Analysis of a spatially evolving direct numerical simulation of a supersonic boundary layer flow at M=2.25," American Physical Society Meeting of the Division of Fluid Dynamics, Dallas, Nov. 24-26, 2002.

Rai, M. M., and Moin, P. 1991 Direct simulations of turbulent flow using finite-difference schemes, *J. Comp. Phys.*, **96**, 15–53.

Rai, M. M. and Moin, P. 1993 "Direct numerical simulation of transition and turbulence in a spatially evolving boundary layer," *J. Comp. Phys.* **109**, 169–192.

Rai, M. M., Gatski, T. B. and Erlebacher, G. 1995 "Direct simulation of spatially evolving compressible turbulent boundary layers," *AIAA Paper 95-0583*.

Sarkar S., 1995 "The stabilizing effect of compressibility in turbulent shear flow," *J. Fluid Mech.* **282**, 163–186.

Sarkar, S., Erlebacher, G., Hussaini, M. Y., and Kreiss, H. O. 1991 "The analysis and modelling of dilatational terms in compressible turbulence," *J. Fluid Mech.* **227**, 473–493.

Shutts, W. H., Hartwig, W. H., and Weiler, J. E. 1977 In: "A critical compilation of compressible turbulent boundary layer data," (Fernholz, H. H. and Finley, P. J., Eds.) *AGARDograph No. 223*.

Smits, A. J. and Dussauge, J.-P. 1996 *Turbulent Shear Layers in Supersonic Flow*, AIP Press.

Spalart, P. R., 1988 "Direct simulation of a turbulent boundary layer up to $Re_\theta = 1410$," *J. Fluid Mech.* **187**, 61–98.

White, F. M. 1974 *Viscous Fluid Flow*, McGraw-Hill.

REPORT DOCUMENTATION PAGE

Public reporting burden for this collection of information is estimated to average 1 hour per response, including the time for reviewing instructions, searching existing data sources, gathering and maintaining the data needed, and completing and reviewing the collection of information. Send comments regarding this burden estimate or any other aspect of this collection of information, including suggestions for reducing this burden, to Washington Headquarters Services, Directorate for Information Operations and Reports, 1215 Jefferson Davis Highway, Suite 1204, Arlington, VA 22202–4302, and to the Office of Management and Budget, Paperwork Reduction Project (0704–0188), Washington, DC 20503.

1. AGENCY USE ONLY *(Leave blank)*	2. REPORT DATE	3. REPORT TYPE AND DATES COVERED
	September 2002	Technical Memorandum

4. TITLE AND SUBTITLE
Numerical Simulation of a Spatially Evolving Supersonic Turbulent Boundary Layer

5. FUNDING NUMBERS
706-31-11-06

6. AUTHOR(S)
T. B. Gatski and G. Erlebacher

7. PERFORMING ORGANIZATION NAME(S) AND ADDRESS(ES)
NASA Langley Research Center
Hampton, VA 23681–2199

8. PERFORMING ORGANIZATION REPORT NUMBER
L–18225

9. SPONSORING/MONITORING AGENCY NAME(S) AND ADDRESS(ES)
National Aeronautics and Space Administration
Washington, DC 20546–0001

10. SPONSORING/MONITORING AGENCY REPORT NUMBER
NASA/TM–2002–211934

11. SUPPLEMENTARY NOTES

12a. DISTRIBUTION/AVAILABILITY STATEMENT
Unclassified-Unlimited
Subject Category 34   Distribution: Nonstandard
Availability: NASA CASI (301) 621–0390

12b. DISTRIBUTION CODE

13. ABSTRACT *(Maximum 200 words)*
The results from direct numerical simulations of a spatially evolving, supersonic, flat-plate turbulent boundary-layer flow, with free-stream Mach number of 2.25 are presented. The simulated flow field extends from a transition region, initiated by wall suction and blowing near the inflow boundary, into the fully turbulent regime. Distributions of mean and turbulent flow quantities are obtained and an analysis of these quantities is performed at a downstream station corresponding to $Re_x = 5.548 \times 10^6$ based on distance from the leading edge.

14. SUBJECT TERMS
Direct Numerical Simulation, Supersonic Flow, Boundary Layer

15. NUMBER OF PAGES
23

16. PRICE CODE

17. SECURITY CLASSIFICATION OF REPORT
Unclassified

18. SECURITY CLASSIFICATION OF THIS PAGE
Unclassified

19. SECURITY CLASSIFICATION OF ABSTRACT
Unclassified

20. LIMITATION OF ABSTRACT

NSN 7540-01-280-5500